

# Experimental Test-Object Study of Electronically Collimated SPECT

Manbir Singh and R. Ricardo Brechner

*Department of Radiology, University of Southern California, Los Angeles, California*

The imaging performance of a prototype electronically collimated single-photon emission computed tomography (SPECT) camera comprising a unique  $4 \times 4$  germanium detector backed by an uncollimated scintillation camera has been evaluated. Three-dimensional images of cylindrical test-objects containing either  $^{99m}\text{Tc}$  (140 keV) or  $^{137}\text{Cs}$  (662 keV) are reported. Electronically collimated counts were acquired from the objects rotated to 20 or 40 angular positions in front of the germanium detector to simulate a cylindrical scanning system. For comparison, mechanically collimated data were also acquired from the test-objects. The SPECT images show a slightly better resolution for mechanical over electrical collimation ( $1.3 \pm 0.25$  cm mechanical,  $1.5 \pm 0.25$  cm electrical at 140 keV;  $1.5 \pm 0.25$  cm mechanical,  $1.7 \pm 0.25$  cm electrical at 662 keV). The equi-resolution sensitivity, however, was deduced to be approximately an order of magnitude higher with electronic collimation to image a head-sized object using  $^{99m}\text{Tc}$ . In addition, the sensitivity gain increases with increasing energy, suggesting the unique potential of electronic collimation in high-energy SPECT.

**J Nucl Med 1990; 31:178-186**

The technique of electronic collimation, first proposed by Singh et al. (1) in 1977 for single-photon emission computed tomography (SPECT), represents an alternative to conventional mechanical collimation for localizing gamma emitters. Most SPECT studies are currently performed with a rotating scintillation camera equipped with a parallel-hole or a similar multi-hole mechanical collimator (2,3). Mechanical collimation suffers from a fundamentally low sensitivity since only a small fraction of gamma rays emitted from the object are transmitted through the apertures to produce counts. Also, in addition to limiting dynamic SPECT studies, rotation of the bulky camera head is a potential source of errors introduced by mechanical unstabilities in the moving parts and changes in the response of the photomultiplier tubes with motion (4). Furthermore, if the energy of the emitted radiation exceeds 250 keV,

the combination of the required septal thickness, length and diameter of the apertures for effective collimation deteriorate the resolution, uniformity and sensitivity to the point where it becomes almost impractical for imaging. Thus, only a limited number of radioisotopes with gamma energies in the 70–200 keV range have been utilized effectively in nuclear medicine and many potentially useful radionuclides either have not been considered or are imaged under suboptimal conditions.

Recently, SPECT systems based on a ring of stationary detectors (5), stationary cameras (6) or a single cylindrical NaI crystal (7) have been designed in conjunction with a rotating collimator. Although these designs overcome the mechanical stability and field uniformity problems associated with the rotating scintillation camera, the basic limitations of sensitivity and high-energy imaging remain similar to a conventional SPECT system. Also, dynamic studies are now constrained by the collimator motion.

To overcome these fundamental drawbacks of a mechanical collimator, an electronically collimated SPECT instrument based on detecting a sequential interaction of the emitted gamma rays with two position- and energy-sensitive detectors has been designed by Singh (8). Counts in electronic collimation are acquired in a coincidence counting mode between two detectors (det1 and det2) from those gamma rays which scatter from det1 onto det2 after depositing a measurable energy in det1. From the physics of Compton scattering, each coincident count originates from activity lying somewhere on a hollow cone whose vertex, axis and angle are known with an accuracy depending on the position and energy resolution of the detectors. Localization of activity, i.e., collimation is thereby achieved electronically upon hollow cones traversing the object. Since each coincident count identifies, in general, a different hollow cone, a very large number of intersecting conical surfaces are generated in a study from which the three-dimensional activity distribution can be reconstructed (9–14).

The design and basic characteristics of an electronically collimated system comprising a  $33 \times 33$  array of small germanium (Ge) detectors as det1 and an uncollimated conventional scintillation camera as det2 have been reported previously (8,15). The basic concept of

Received Apr. 13, 1989; revision accepted Oct. 3, 1989.  
For reprints contact: Manbir Singh, PhD, Associate Professor of Radiology, University of Southern California, Health Sciences Campus, PSC-610, 1985 Zonal Avenue, Los Angeles, CA 90033.

electronic collimation is illustrated in Figure 1. Considering a single element from the det1 array and an on-axis point source as shown in Figure 1, the coincident counts on det2 will form circles with radii proportional to the scattering angle and the separation between det1 and det2. Off-axis point sources, however, will not trace circles but elliptical or partial elliptical profiles representing an intersection of a tilted hollow cone with the planar det2 surface. Thus, the point spread function (PSF) at a specified scattering angle, defined in terms of the coincident count profile on det2, is spatially variant, and the coincident counts from an object at a given scattering angle may be represented as a convolution of the cone-beam projection of the object (where the cone-beam projection is the same as a pin-hole projection image) with a spatially variant PSF (12). Consequently, the cone-beam projection of the object may be recovered by deconvolving the PSF as a function of the known scattering angles. The deconvolution operation is greatly facilitated by mapping the coincident counts on a spherical surface centered on the det1 element under consideration (12).

After deconvolution, a cone-beam projection of the object is obtained from each element of det1. Since det1 is composed of a large number of elements, on the order of 1000, a large number of cone-beam projections from multiple angles of view are obtained simultaneously. These cone-beam projections from multiple angles of view can then be used to reconstruct a three-dimensional image of the object (9,13). Although the design of the original electronically collimated system called for a single  $33 \times 33$  Ge array (8), representing a limited angular sampling instrument, later designs have considered orthogonal and cylindrical geometries to achieve 180- and 360-degree angular sampling, respectively (13). Thus, a totally stationary cylindrical scan-

ning instrument for SPECT could be realized with electronic collimation.

To that end, we have implemented a small prototype electronically collimated system comprising a  $4 \times 4$  array of specially fabricated Ge detectors as det1 and an uncollimated Pho/Gamma IV scintillation camera as det2. The first experimental results of three-dimensional imaging with the prototype system using test objects filled with either  $^{99m}\text{Tc}$  (140 keV) or  $^{137}\text{Cs}$  (662 keV) are reported in this paper.

## MATERIALS AND METHODS

The Ge detector was fabricated from a single high-purity Ge slab, segmented into 16 independent 5 mm x 5 mm x 6 mm elements, and housed in a special liquid nitrogen cryostat with wide entrance and exit windows (16). A photograph of the prototype system with the Ge detector situated in front of the uncollimated scintillation camera is shown in Figure 2. The distance between the Ge detector and the scintillation camera was kept at 5 cm for all experiments reported in this paper. Each Ge element was interfaced to its own amplification, energy discrimination and analog to digital conversion (ADC) circuitry to provide an independent timing and digital energy signal (15,16). The full-width-at-half-maximum (FWHM) energy resolution of the Ge detectors was 850 eV at 140 keV, with less than 10% inter-element variation. The intrinsic spatial resolution of the scintillation camera was 5 mm FWHM for normally incident gamma rays, and its energy resolution was 15% FWHM at 140 keV. The coincidence timing resolution between the Ge detector and the scintillation camera was 100 ns (FWHM) for imaging  $^{99m}\text{Tc}$  and 50 ns (FWHM) for imaging  $^{137}\text{Cs}$  sources. A special microcomputer-based circuit was developed to acquire coincident counts. Detection of a valid coincidence event between the scintillation camera and any element of the Ge detector initiated digital conversion of the x and y position signals in the scintillation camera, identified the Ge element in which the interaction occurred, and digitized the energy deposited within

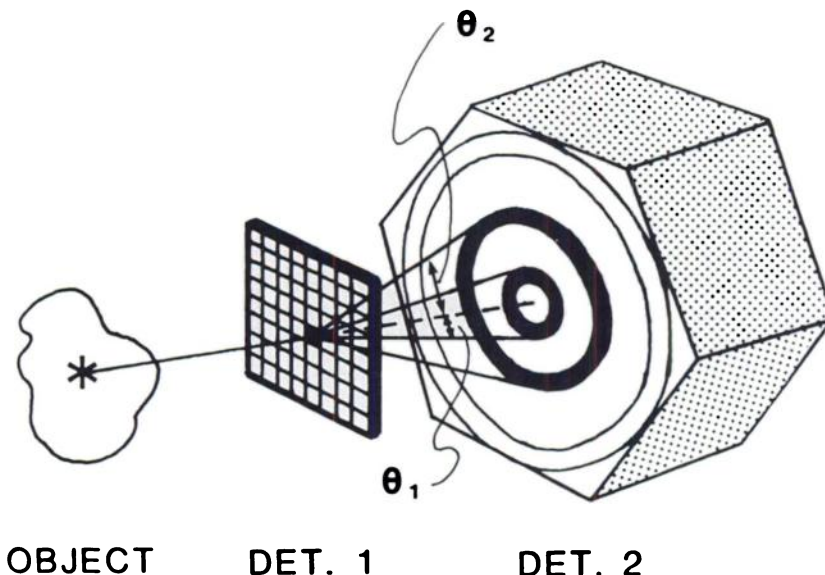


**FIGURE 1**

A depiction of the concept of electronic collimation based on detection of gamma rays scattered from an array of Ge detectors (det1) onto an uncollimated scintillation camera (det 2). Counts are recorded in coincidence between det1 and det2 for events where a small amount of the emitted photon's energy is deposited in det1 and the remaining energy is absorbed in det2. The energy deposited in det1 determines the angle at which gamma rays are scattered from the Ge detector ( $\theta_1$  or  $\theta_2$  in the figure).

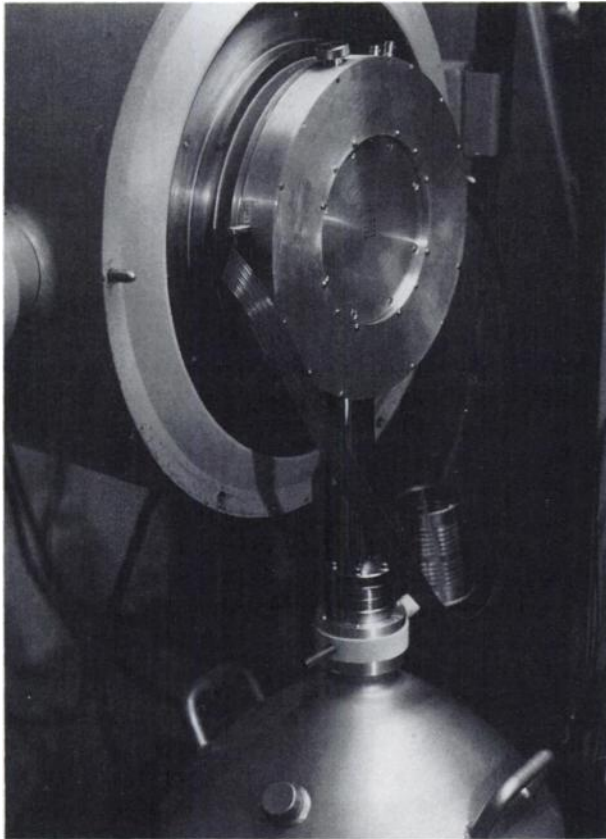


**FIGURE 2**

A photograph of the prototype electronically-collimated camera comprising a  $4 \times 4$  germanium detector enclosed in a liquid nitrogen cooled cryostat situated in front of an uncollimated conventional scintillation camera.

the Ge element to provide a measure of the scattering angle. The event was rejected if more than one Ge element produced a signal simultaneously, thereby removing most of the contribution from Ge inter-element scattering. The coincident counts were framed on-line into  $128 \times 128$  scintillation camera images as a function of the scattering angle in each Ge element. Counts were acquired for scattering angles ranging from approximately  $32^\circ$  to  $56^\circ$  and binned on-line in approximately two-degree wide scattering intervals.

#### **Technetium-99m Test Object Imaging**

A 10-cm diameter cylindrical vessel containing an inner 3-cm diameter hollow cylinder was used as a test object to evaluate the three-dimensional imaging capability of electronic collimation at 140 keV. The vessel was filled to a height of 2 cm with water containing uniformly distributed  $0.7 \mu\text{Ci/cc}$  of  $^{99\text{m}}\text{Tc}$ . The inner cylinder was filled with water containing no activity to form a cold region amidst a uniform background. The object was placed on a rotating platform with its center (which coincided with the center of rotation) at a distance of 12 cm from the Ge detector and rotated to 20 equiangular positions around  $360^\circ$ . At each angle of view, coincident counts were acquired from 10 elements of the  $4 \times 4$  Ge detector and binned on-line in approximately two-degree intervals as mentioned earlier. The total activity in the object

and the resulting coincidence countrate were necessarily low to keep the "singles" count rate on the uncollimated scintillation camera below 20K cps since unacceptable distortions in the camera positioning circuitry were observed above that level in the scintillation camera at hand. Approximately 200K counts were acquired at each angle of view per Ge element at an initial average counting rate of 8.5 cps per element. Three-dimensional images were reconstructed in a  $50 \times 50 \times 25$  volume with 0.5 cm voxels using a two-stage iterative algorithm described elsewhere (12,13). No attenuation or scatter correction was used in these studies.

The Ge detector was then removed and a conventional high resolution parallel-hole collimator designed for  $^{99\text{m}}\text{Tc}$  was mounted on the scintillation camera. Conventional SPECT data were acquired from the same test object (after increasing the  $^{99\text{m}}\text{Tc}$  activity concentration by a factor of 25 to increase the counting rate) at the same radius of rotation (measured from the front surface of the collimator) from 20 equispaced angular views around  $360^\circ$ . The counting time per view was increased to compensate for the decay of  $^{99\text{m}}\text{Tc}$  during data acquisition. Two sets of SPECT data with initial counting times of 1 min and 5 min per projection provided approximately 200K and 1M counts per projection, from where transaxial images were reconstructed using the standard Shepp and Logan algorithm (17) without any attenuation or scatter correction. The central two or four rows in each projection were summed to study the effect of statistics on noise propagation. For reference, a top-view of the object was also acquired by placing the scintillation camera directly on top of the object.

Two measures of the signal-to-noise ratio (SNR), labeled SNR1 and SNR2, were used to compare the imaging performance of electronic and mechanical collimation. SNR1 was defined as the ratio of the mean to the standard deviation in the uniform background portion of the reconstructed images. SNR2 was defined by the product: [contrast  $\times$  SNR1], with contrast defined as  $(B-C)/B$ , where B and C represent mean counts within the uniform portion of the background and within the cold region respectively. In each case, the value of SNR was averaged over multiple slices to obtain a single value for each set of three-dimensional images.

Using count rate as a basis, a comparison of the sensitivities of electronic and parallel-hole collimation was performed to image volume sources of  $^{99\text{m}}\text{Tc}$ . To be consistent with theoretical computations (8), a homogeneous distribution of  $^{99\text{m}}\text{Tc}$  within cylinders, where the diameter of each cylinder was equal to its length, was used. The count rate was measured from three cylinders whose diam  $\times$  length were 5 cm  $\times$  5 cm, 7.8 cm  $\times$  7.8 cm and 11.6 cm  $\times$  11.6 cm, respectively, using all 16 Ge elements in the electronic mode and the high-resolution parallel-hole collimator in the conventional mode. The proximal surface of each cylinder was at a distance of 4.5 cm from the Ge detector or the collimator. Counts in the conventional mode were acquired with a 20% window centered on the photopeak. In the electronic mode, the energy signals from the Ge detector and the scintillation camera were first added and then passed through the same 20% window to ensure that the ratio of primary to scattered photons originating from the object was approximately equal in both modes. The count rate measured with the  $4 \times 4$  Ge detector was extrapolated to estimate the countrate of a  $33 \times 33$  Ge detector

system for comparing the experimental values with the theoretical values of the sensitivities of an electronically and a mechanically collimated system reported previously (8).

### Cesium-137 Test Object Imaging

A 15-cm diameter cylindrical vessel containing an inner 2.5 cm diameter hollow cylinder (to form a hot region) and two solid lucite cylinders of diameters 3.0 cm and 2.0 cm, respectively, (to form cold regions) was used to investigate the three-dimensional imaging performance of electronic collimation at a high gamma energy of 662 keV. The vessel was filled to a height of 2 cm with 0.2  $\mu\text{Ci/cc}$  of  $^{137}\text{Cs}$ . The hollow inner cylinder was filled with 2.0  $\mu\text{Ci/cc}$ . Coincident data were acquired from 40 equispaced angular views around 360° using 10 Ge elements and 12 scattering windows per element, where each window was approximately two degrees wide as mentioned earlier. The center of the test object coincided with the center of rotation and was at a distance of 14.5 cm from the Ge detector. An average of 67K counts were acquired per Ge element per angle of view, at an average rate of 2 cps per element.

The Ge detector was then replaced by a 5-mm diameter lead pin-hole collimator, and counts were acquired over 40 angles of view as above with the center of the object located 14.5 cm from the pin-hole. The concentration of activity in the background and the hot region was doubled to increase the counting rate with the mechanically collimated scintillation camera. Data were acquired for 1, 2, 4, 8 and 15 min of counting per view, yielding a total (combined from all views) of 90, 192, 352, 730, and 1480K counts for reconstructing the central cross-section. After mapping onto a spherical surface, images were reconstructed from these data using the same ART algorithm as used in the second stage of the electronically collimated reconstruction. The SNRs in the electronically and mechanically collimated images were then compared in the reconstructed central cross-sections using SNR1 and SNR2 defined earlier.

## RESULTS

The electronically collimated  $^{99\text{m}}\text{Tc}$  test object three-dimensional images, reconstructed from 20 views on

0.5 cm contiguous transaxial slices are shown in Figure 3. The resolution at the 12 cm center of rotation was measured with a  $^{99\text{m}}\text{Tc}$  line source to be  $1.5 \pm 0.25$  cm. The electronic and parallel-hole collimated images are compared in Figure 4. A central level transaxial reconstruction from 20 views containing the same number of total counts (1.1M) in each case, is shown. The electronically collimated image is shown at the left, the parallel-hole collimated image in the center, and the top-view of the object representing the best possible transaxial image obtainable with the scintillation camera used in these studies, is shown at the right. The spatial resolution in the conventional SPECT image was measured with a  $^{99\text{m}}\text{Tc}$  line source to be  $1.3 \pm 0.25$  cm. For comparison, profiles through the cold region are also shown in Figure 4.

Plots of the SNR1 and SNR2 in electronic and conventional SPECT images as a function of the total number of acquired counts over 20 angular views are shown in Figure 5. Assuming that the SNR is directly proportional to the transaxial resolution for a given slice thickness, the SNR in mechanical collimation, as plotted in Figure 5, was increased by the factor 1.5/1.3 from its measured value to compensate for the slightly lower resolution of electronic collimation. These plots indicate an average SNR1 (electronic)/SNR1 (mechanical) value of 0.8 and an average SNR2 (electronic/mechanical) value of 0.78 to reconstruct equi-resolution SPECT images from the same number of counts.

The count rate-based sensitivity comparison of an electronic and parallel-hole collimated system is summarized in Table 1. The first column lists the diameter of the cylindrical vessels (the diameter and length of each cylinder are equal). The next two columns show the computed sensitivity gain for electronic over parallel-hole collimation for object distances (proximal surface) of 1.0 and 4.5 cm, respectively, if a large-field-of-view (LFOV) scintillation camera, which has a 40-cm

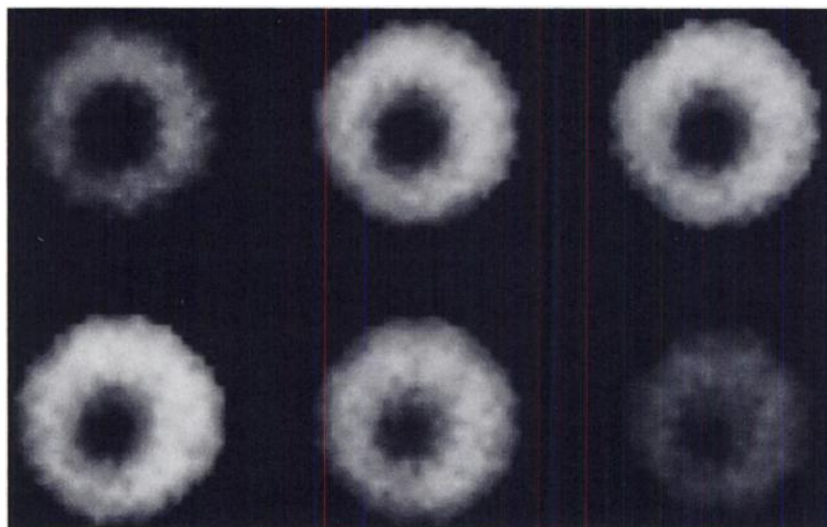
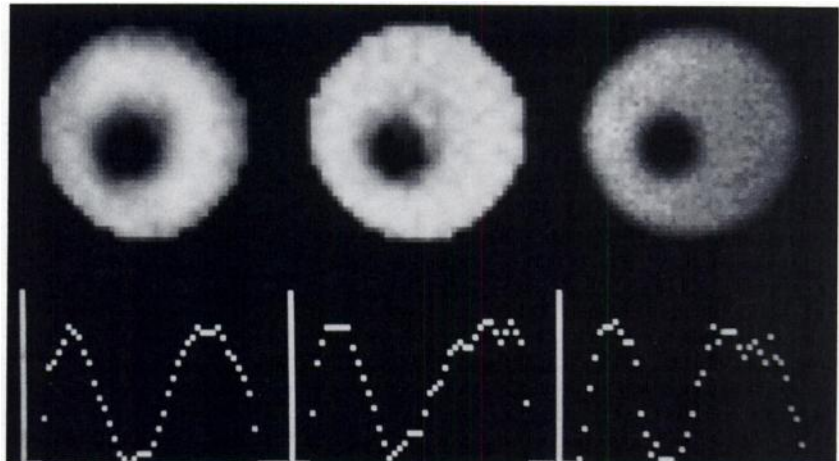


**FIGURE 3**

Technetium-99m test-object imaging with electronic SPECT. Contiguous 0.5-cm transaxial planes through the object containing a uniform activity distribution of  $^{99\text{m}}\text{Tc}$  and an inner cold region are shown. These images were reconstructed with a two-stage ART algorithm using data acquired with the prototype electronically-collimated system from 20 equispaced angular locations of the germanium detector around 360°. Contiguous slices, starting from the bottom of the object, are arranged from left to right in this figure. The inner cold cylinder was flared at the bottom as visualized in the top left image.

**FIGURE 4**

A comparison of the electronic (left) and conventional mechanical (center) transaxial SPECT images of the <sup>99m</sup>Tc object containing an equal number of acquired counts (1.1 M) in each case. The electronic image is a central cross-section taken from Figure 3. The conventional image is a central level cross-section reconstructed from data acquired from 20 angles of view around 360° using a parallel-hole collimated scintillation camera and a standard filtered backprojection algorithm. A top view of the object, acquired by placing the parallel-hole collimator directly on top of the object is shown at the right. All of these images are shown on 0.5 cm × 0.5 cm pixels. A profile through the cold region is shown at the bottom, indicating very similar resolution and contrast recovery for electronic and mechanical collimation.



diameter planar crystal, were used in both systems. (The electronic system is assumed to comprise a 33 × 33 Ge detector for this comparison.) The fourth and fifth columns show respectively theoretical and experimental results for the 20-cm diameter scintillation camera used in the prototype system, with an object distance of 4.5 cm.

The reconstructed three-dimensional images of the <sup>137</sup>Cs test object from a total of 13M counts acquired over 40 angles of view are presented in Figure 6. The images are shown as 0.5-cm thick contiguous transaxial slices. The spatial resolution in these images, as measured from the three-dimensional reconstruction of data acquired from an off-center point source with the same

center of rotation as the test object, was  $1.7 \pm 0.25$  cm. A central cross-section of the object, reconstructed from two Ge detection elements with a relatively low number of total acquired counts (860K), is shown at the left in Figure 7, and the reconstruction at the same central level using mechanical pin-hole collimation with approximately the same number of total acquired counts (730K) is shown at the right. The spatial resolution in the mechanically collimated images was measured to be  $1.5 \pm 0.25$  cm. The equi-resolution SNR (electronic)/SNR (mechanical) values corresponding to a total of 500K, 1M and 1.5M acquired counts in each modality were 0.70, 0.69 and 0.66 respectively for SNR1 and 0.66, 0.70 and 0.71 respectively for SNR2.

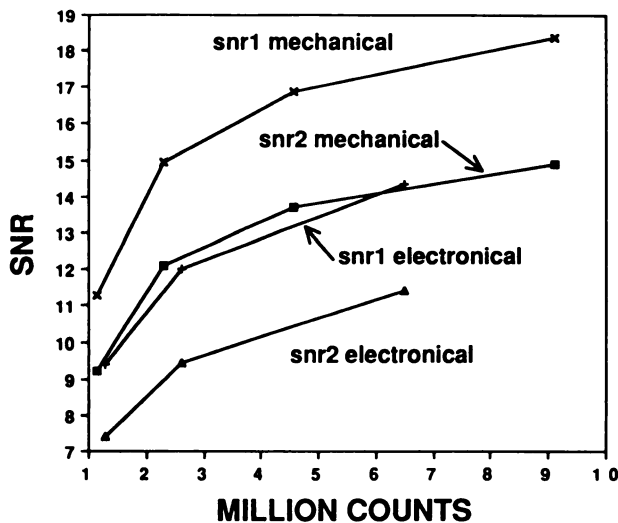


**FIGURE 5**

A comparison of the signal-to-noise ratio (SNR) using two definitions (SNR 1 and SNR 2) described in the text. Plots are shown for mechanical and electronic images of the <sup>99m</sup>Tc test-object as a function of the total counts in each case.

**TABLE 1**  
Theoretical and Experimental Sensitivity Gains for Electronic over Mechanical Collimation Based on <sup>99m</sup>Tc Count Rate as a Function of Object Size

L cm	Theoretical			Exp
	d = 1 cm LFOV	d = 4.5 cm LFOV	d = 4.5 cm Pho/G	d = 4.5 cm Pho/G
5.0	300	80	58	63
7.8	149	58	42	39
10.0	100	46	33	
11.6	78	40	29	28
15.0	50	30	22	
20.0	30	21	15	
25.0	20	16	12	

L = length and diameter of cylindrical objects; d = distance of proximal surface of object from collimator or the Ge detector; LFOV = large-field-of-view scintillation camera with a 40-cm diameter useful crystal region.

Pho/G denotes 20-cm diameter scintillating camera used in electronically-collimated prototype.

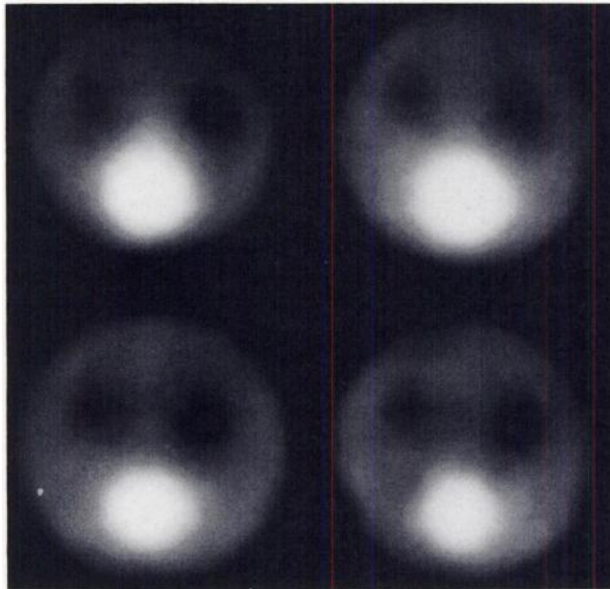


**FIGURE 6**  
Tomographic images of the  $^{137}\text{Cs}$  object containing hot and cold regions amidst a uniform background, reconstructed on  $0.5\text{ cm} \times 0.5\text{ cm}$  pixels, within 0.5-cm thick contiguous transaxial planes. A total of 8.6 M coincident counts, acquired from 40 equispaced angular locations over  $360^\circ$ , were used to reconstruct the shown set of tomographic images. The resolution in these images, corresponding to a 14.5-cm radius of rotation, was measured to be  $1.7 \pm 0.25\text{ cm}$ .

## DISCUSSION

The three-dimensional images shown in this paper represent the results of “first experiments” performed with the prototype electronically collimated SPECT instrument, and as such, are expected to improve with

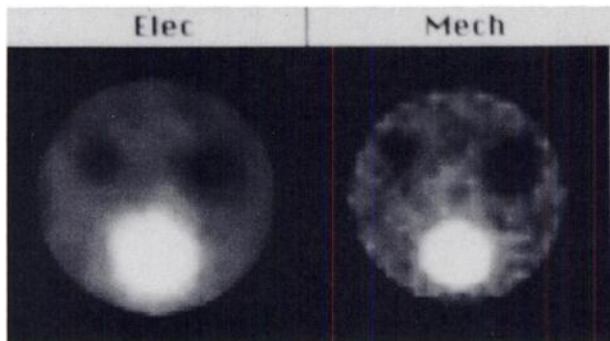


**FIGURE 7**  
A relatively low-count transaxial image of the  $^{137}\text{Cs}$  object, reconstructed from a total of 860K electronically collimated counts acquired over 40 angles of view is shown at left, and a mechanically (pin-hole) collimated transaxial image at the same level of the object, reconstructed from approximately the same number of acquired total counts (730K) over 40 angles of view, is presented at right. The mechanically-collimated image shows a slightly better resolution ( $1.5 \pm 0.25\text{ cm}$ ), compared to the electronically-collimated image ( $1.7 \pm 0.25\text{ cm}$ ).

better detectors, electronics and image reconstruction algorithms in future systems.

The experimentally measured resolution can be compared with theoretical predictions derived from the procedure described elsewhere (8). For example, in  $^{99\text{m}}\text{Tc}$  imaging, if we assume a two-degree FWHM resolution in determining the scattering angle and a 5-mm intrinsic resolution for normal incidence on the scintillation camera, theory predicts a line spread function (LSF) of 1.38 cm at 12 cm, which is in reasonably good agreement with the experimental value of  $1.5 \pm 0.25\text{ cm}$ . The theoretical value at a distance of 10 cm from the detector is 1.1 cm for a 5-cm separation (as used in these studies) between the Ge detector and the scintillation camera. If the inter-detector separation were increased to 10 cm, the resolution would improve to 0.69 cm. However, the sensitivity would now drop to 0.73 of the value at the 5-cm inter-detector separation. The sensitivity decrease could be recovered by increasing the area of the scintillation camera (or cameras) to maintain the detection solid angle between the Ge detector and the scintillation camera.

The prototype system described here was designed to perform initial feasibility studies and utilized an existing scintillation camera. A conventional planar scintillation camera, however, is inadequate as the second detector of a practical electronically collimated system since it is unable to operate properly at the very high “singles” rate expected in clinical imaging (8). In practice, therefore, the conventional camera must be replaced by a group of small independent modular cameras where each modular camera would operate at an order of magnitude higher count rate over our existing scintillation camera (i.e., 200K cps vs 20K cps). At least two versions of small modular scintillation cameras suited for electronic collimation are currently under development (18,19). It is expected that these cameras will become available commercially in the near future at a cost, based on per unit detection area, comparable to conventional scintillation cameras.

Since the scintillation light in a NaI(Tl) crystal is emitted with a decay time of 240 ns, a 1- $\mu\text{sec}$  pulse integration time is normally used to collect 98% of the emitted light. At 200K cps, a 1- $\mu\text{sec}$  integration time will result in a crystal deadtime of slightly under 20%, with a corresponding reduction in the sensitivity of the electronically collimated system to approximately 80% of its full value. However, the deadtime could be reduced to under 10% at 200K cps with minimal loss in the energy or position resolution in the scintillation camera by narrowing the scintillation pulse and using a shorter or variable pulse integration time (20). In addition, much higher count rates could be accommodated by implementing digital position encoding. For example, using a short pulse integration time of 240 ns in conjunction with pulse clipping and digital position

estimation, measurements of count rates as high as 2M cps have been reported recently with a 20% maximum deadtime and a 20% degradation in the FWHM position resolution (21).

Small modular cameras are not available to us at the present time. The present work was carried out with an existing 20-cm diameter conventional camera with limited count rate capabilities, forcing us to confine our measurements to relatively small test-objects containing very low activity and consequently requiring very long counting times. To maximize the coincident count rate with the available instrumentation, the Ge detector and the scintillation camera were separated by a relatively short distance of 5 cm, thereby increasing the sensitivity at the expense of spatial resolution.

The coincidence temporal window and the "singles" count rate on both detectors (Ge and the scintillation camera) determine the rate of random coincident counting. The width of the coincidence window is usually set at twice the FWHM coincidence timing resolution to capture 98% of the coincident events. At a given timing resolution, narrowing the coincident window improves the ratio of true-to-random coincident counts, albeit at the expense of system sensitivity. For example, reducing the window width by a factor of two would double the true-to-random ratio but reduce the sensitivity to 76% of its initial value. Improvements in the timing resolution, on the other hand, would enable higher true-to-random ratios to be achieved without sacrificing sensitivity. Since photons are scattered from the Ge detector after depositing a relatively small energy, the timing resolution attainable in the Ge detector is the main limiting factor in improving the coincident timing resolution. The timing resolution improves with the energy of the primary photons since more energy is deposited in the Ge detector. The timing resolutions reported here (100 ns for  $^{99m}\text{Tc}$ , 50 ns for  $^{137}\text{Cs}$ ) were obtained by a relatively straightforward zero cross-over technique (16) and should be adequate in practical imaging. For example, it is estimated that 0.1  $\mu\text{Ci/cc}$  of  $^{99m}\text{Tc}$  uniformly distributed within a 20-cm diameter  $\times$  20-cm tall cylinder would yield a true to random ratio of about six with a 200-ns wide coincidence temporal window (15). Better timing resolution, which would be desirable in imaging higher activity concentrations, could be realized with a thinner Ge detector or by raising the threshold for recording the minimum scattering angle in the Ge detector, both at the expense of system sensitivity (8).

The count rate-based sensitivity comparison between electronic and parallel-hole collimation indicates more than an order of magnitude advantage for electronic over parallel-hole collimation. For example, assuming a  $33 \times 33$  Ge detector and a 40-cm diameter scintillation camera, a factor of 30 gain in sensitivity is indicated for imaging a 20-cm diameter  $\times$  20-cm long cylindrical

distribution of  $^{99m}\text{Tc}$ , where the proximal surface of the cylinder is located 1 cm from the Ge detector. In actual experiments with the prototype, the objects could not be placed closer than 4.5 cm due to mechanical constraints (which will be corrected in future designs). Also, the prototype utilized a 20-cm diameter scintillation camera. The experimentally measured sensitivity gains with the existing prototype are therefore lower than those that could be realized in future systems. Nonetheless, the experimentally measured gain of, e.g., a factor of 28 for imaging a 11.6-cm diameter  $\times$  11.6-cm long cylindrical distribution of  $^{99m}\text{Tc}$  (obtained after extrapolating counts measured with the  $4 \times 4$  prototype to counts that would be measured with a  $33 \times 33$  Ge detector) represents a very significant improvement in the counting sensitivity.

Unlike conventional SPECT where activity is localized on lines or "ray sums" (22) through the object, electronic collimation localizes counts on conical surfaces, i.e., each count represents the sum of activity lying on a conical surface traversing the object. The first stage of the two-stage reconstruction algorithm reduces the localization uncertainty by processing the acquired counts to generate ray-sums through the object. At the end of the first stage of the reconstruction procedure, cone-beam views of the object are obtained for each element of the Ge detector. These cone-beam views from multiple angles of view are then combined in the second stage of the reconstruction algorithm to produce three-dimensional images. Thus, the second stage of the reconstruction algorithm is similar to conventional SPECT where three-dimensional images are reconstructed from two-dimensional cone-beam projections. However, the first stage of the reconstruction algorithm is unique to electronic collimation and introduces extra noise in the image reconstruction process. This extra noise must be accounted for to determine the effective sensitivity increase of electronic over conventional collimation.

Noise propagation in the first stage of the reconstruction algorithm has been studied by theoretical, computer simulation and experimental studies as described in a previous publication (23). Briefly, the approaches investigated include:

1. A theoretical analysis using an approximate description of the scattering PSF in the form of an annulus.
2. Inverse Fourier filtering of a simulated disk source containing hot and cold regions.
3. Deconvolution of computer-simulated data on a spherical surface using the first-stage iterative algorithm.
4. Experimental reconstruction of a 5-cm diameter  $^{137}\text{Cs}$  disk source.

These studies indicate that the effective sensitivity of electronic collimation would be reduced by a factor of two to three due to noise propagation in the first stage

of the reconstruction procedure. It should be noted that the first stage projection image is reconstructed from data acquired over many ( $\sim 12$ ) scattering angles, sampled on a sufficiently large scintillation detector area. Each scattering angle provides an independent  $N \times N$  data set for reconstructing the common  $N \times N$  projection image. Thus, the reconstruction problem is "well-conditioned," enabling an unambiguous estimation of the projection image. Indeed, we have not encountered any systematic errors in our first stage reconstruction studies so far.

The experimental test-object images presented here provide a verification of the noise propagation studies and allow us to estimate the gain in the effective sensitivity of electronic collimation for larger objects. Since cone-beam projection images are reconstructed in the first stage by deconvolving an annular PSF, the noise in the first stage is expected to be a function of the projected area of the object and not its volume. Noise in the second stage depends on the depth or thickness of the object as well, making the combined noise from both stages dependent on the volume of the object. However, we are assuming that the noise propagation in the second stage of electronic collimation is similar to the noise propagation in mechanically collimated SPECT. Thus, the extra noise in electronic collimation, attributed to the first stage, is primarily a function of the projected object area, and studies performed with disk sources may be used to study this additional noise as a function of object size. An analytic expression for noise propagation in annular coded aperture imaging, which is very similar to the first stage reconstruction in electronic collimation, has been derived by Barrett (24), indicating that the SNR is proportional to  $1/A^{1/4}$ , where  $A$  is the area of a disk source. The SNR in (24) relates to SNR1 in the present work.

Using a plane through the center of rotation as a reference for computing the projected areas, the  $^{99m}\text{Tc}$  object has an area of  $\sim 20 \text{ cm}^2$ , and the  $^{137}\text{Cs}$  object an area of  $\sim 30 \text{ cm}^2$ . The average ratios of SNR1 (electronic) to SNR1 (mechanical) for these objects are 0.8 and 0.68, respectively. These values are consistent with a  $1/A^{1/4}$  dependence and may be used to estimate the SNRs for imaging larger objects since actual measurements of larger objects must await completion of the next version of an electronically collimated system based on modular scintillation cameras. Extrapolating the measured values we find that the relative SNR1 (electronic/mechanical) for imaging a 22-cm diameter  $\times$  10-cm object resembling a head section, for example, would be equal to 0.43. Smaller values would be obtained for larger objects.

The relative SNRs provide a means for determining the effective sensitivity gain of electronic over mechanical collimation. Assuming that the SNR is proportional to the square root of acquired counts, the experimen-

tally measured SNRs for the two test-objects suggest that to achieve equal SNRs with electronic and mechanical collimation in the final reconstructed images, a factor of 1.6 more counts must be acquired with electronic compared to mechanical collimation for the measured  $^{99m}\text{Tc}$  object and a factor of two more counts for the  $^{137}\text{Cs}$  object. Also, the sensitivity gains listed in Table 1 must be reduced proportionately to arrive at the effective sensitivity gain in three-dimensional imaging. For example, assuming the gain listed in Table 1 for a 15-cm diameter  $\times$  15-cm tall cylinder to be a good representation of the 22-cm diameter  $\times$  10-cm head section mentioned above (based on projected areas), the effective sensitivity advantage of electronic collimation would be reduced by approximately a factor of five. Still, an order of magnitude gain in the effective sensitivity of electronic over mechanical collimation could be realized in this situation for imaging with  $^{99m}\text{Tc}$ , representing a significant advance in SPECT instrumentation. The sensitivity advantage would decrease for larger objects in proportion to the  $1/A^{1/4}$  dependence of noise and the sensitivity gains listed in Table 1.

Higher sensitivity gains are expected with increasing gamma energy (25). For example, theoretical computations show that the count rate based sensitivity of electronic collimation at 500 keV to image a 20-cm diameter  $\times$  20-cm tall cylindrical distribution would be almost three orders of magnitude higher than parallel-hole collimation. This dramatic gain in the relative sensitivity of electronic collimation is based on two factors: 1) a sharp reduction in the sensitivity of a close-packed parallel-hole collimator as a function of energy since thicker septa are required at higher energies, and 2) a gradual increase in the sensitivity of electronic collimation with energy due to an increase in the Compton/photoelectric ratio and more forward scattering at higher energies (8).

The absolute sensitivity of electronic collimation at higher energies is dependent on the absorption efficiency of the scintillation camera. The  $^{137}\text{Cs}$  source imaging reported here was performed with a 0.5-in. thick NaI crystal which has an absorption efficiency of only  $\sim 0.1$  at 662 keV and 0.15 at 500 keV, compared to  $\sim 0.9$  at 140 keV. Although the probability of Compton scattering and subsequent incidence on the scintillation camera increases by a factor of two at 662 keV compared to 140 keV (8), the lower absorption efficiency for  $^{137}\text{Cs}$  results in approximately a factor of four lower count rate for the  $^{137}\text{Cs}$  object after accounting for the total activity in both objects. If a scintillation material such as BGO were used in the scintillation camera to approach an absorption efficiency of 100% for  $^{137}\text{Cs}$ , the sensitivity of electronic collimation at 662 keV would be about a factor of two higher than at 140 keV.

In conclusion, we have presented electronically collimated SPECT images of test-objects containing either  $^{99m}\text{Tc}$  or  $^{137}\text{Cs}$ , demonstrating the versatility and potential of electronic collimation in imaging radiopharmaceuticals covering a wide range in gamma energies. Our results suggest that at equal resolution, the sensitivity of an electronically collimated scintillation camera would be approximately an order of magnitude higher than the sensitivity of the same scintillation camera with parallel-hole collimation for imaging a 22-cm diameter  $\times$  10-cm head-sized section using  $^{99m}\text{Tc}$ . (In practice, a group of small modular scintillation cameras instead of the conventional scintillation camera is required in electronic collimation.) The sensitivity advantage decreases with increasing object size. Unlike conventional collimation, however, where the sensitivity decreases rapidly with energy, the sensitivity of electronic collimation increases with energy, suggesting that electronic collimation would be particularly suited to high-energy SPECT. An immediate application of electronic collimation would be in imaging  $^{131}\text{I}$ -labeled monoclonal antibodies with a higher sensitivity and resolution than possible with conventional collimation. New radiopharmaceuticals labeled with high-energy gamma emitting radionuclides could be developed in the future to achieve better labeling and half-life characteristics.

#### ACKNOWLEDGMENT

This investigation was supported by Grant No. 2 RO1 CA28105-09, awarded by the National Cancer Institute, DHHS. Partial support was obtained from Grant No. FG03-84ER60219, awarded by the Department of Energy.

The authors are grateful to F. Goulding, R.H. Pehl, D.A. Landis, N.W. Madden, P. Luke, D.F. Malone, and C.P. Cork of the Lawrence Berkeley Laboratory, University of California, for their invaluable contributions to the design and fabrication of the germanium detector.

#### REFERENCES

- Singh M, Gustafson DE, Berggren MJ, Gilbert BK, Ritman EL. Physics of electronic collimation for single photon transaxial tomography. *Med Phys* 1977; 4:350.
- Budinger TF. Physical attributes of single-photon tomography. *J Nucl Med* 1980; 21:579-592.
- Jaszczak RJ, Greer KL, Floyd CE, Manglos SH, Coleman RE. Imaging characteristics of a high resolution cone beam collimator. *IEEE Trans Nucl Sci* 1988; NS-35(1):644-648.
- Rogers WL, Clinthorne NH, Harkness BA, Koral KF, Keyes JW. Fieldflood requirements for emission computed tomography with an Anger camera. *J Nucl Med* 1982; 23:162-168.
- Chang W, Tsui BMW, Tian Z, et al. Design and investigation of a modular focused collimator based multiple detector ring system for SPECT imaging of the brain. *SPIE* 1986; 671:200-205.
- Rogers WL, Clinthorne NH, Shao L et al. SPRINT II: A second generation single photon ring tomograph. *IEEE Trans Med Imag* 1988; 7:291-297.
- Genna S, Smith AP. The development of ASPECT, an annular single crystal brain camera for high efficiency SPECT. *IEEE Trans Nucl Sci* 1988; NS-35(1):654-658.
- Singh M. An electronically collimated gamma camera for single photon emission computed tomography. Part I: Theoretical considerations and design criteria. *Med Phys* 1983; 10:421-427.
- Singh M, Doria D. An electronically collimated gamma camera for single photon emission computed tomography. Part II: Image reconstruction and preliminary experimental measurements. *Med Phys* 1983; 10:428-435.
- Singh M, Doria D. Computer simulation of image reconstruction with a new electronically collimated gamma tomography system. *SPIE* 1981; 273:192-200.
- Doria D, Singh M. Comparison of reconstruction algorithms for an electronically collimated gamma camera. *IEEE Trans Nucl Sci* 1982; NS-29(1):447-451.
- Brechner R, Singh M. Reconstruction of electronically collimated images obtained from single gamma emitters using a spherical system of coordinates. *IEEE Trans Nucl Sci* 1986; NS-33(1):583-586.
- Brechner R, Singh M, Leahy R. Computer simulated studies of tomographic reconstruction with an electronically collimated camera for SPECT. *IEEE Trans Nucl Sci* 1987; NS-34(1):369-373.
- Hebert T, Leahy R, Singh M. Maximum likelihood reconstruction for a prototype electronically collimated single photon emission system. *SPIE* 1987; 767:77-83.
- Singh M, Doria D. Single photon imaging with electronic collimation. *IEEE Trans Nucl Sci* 1985; NS-32(1):843-847.
- Pehl RH, Maden NW, Landis DA, Malone DF, Cork CP. Cryostat and electronic development associated with multi-detector spectrometer system. *IEEE Trans Nucl Sci* 1985; NS-32(1):22-28.
- Shepp LA, Logan BF. The Fourier reconstruction of a head section. *IEEE Trans Nucl Sci* 1974; NS-21(3):21-43.
- Milster TD, Selberg LA, Barrett HH, et al. A modular scintillation camera for use in nuclear medicine. *IEEE Trans Nucl Sci* 1984; NS-31(1):578-580.
- Kume H, Muramatsu S, Iida M. Position sensitive photomultiplier tubes for scintillation imaging. *IEEE Trans Nucl Sci* 1986; NS-33(1):359-363.
- Karp JS, Muehllehner G, Beerbohm D, Mankoff DA. Event localization in a continuous scintillation detector using digital processing. *IEEE Trans Nucl Sci* 1985; NS-33(1):550-555.
- Mankoff DA, Muehllehner G, Karp JS. The effect of detector performance on high count rate PET imaging with a tomograph based on position-sensitive detectors. *IEEE Trans Nucl Sci* 1988; NS-35(1):592-597.
- Budinger TF, Gullberg GT. Three-dimensional reconstruction in nuclear medicine emission imaging. *IEEE Trans Nucl Sci* 1974; NS-21(3):2-20.
- Singh M, Leahy R, Brechner R, Hebert T. Noise propagation in electronically collimated single photon imaging. *IEEE Trans Nucl Sci* 1988; NS-35(1):772-777.
- Barrett HH, Swindell W. Noise in radiographic images. In: Barrett HH, Swindell W, eds. *Radiological imaging: The theory of image formation, detection, and processing. Volume 2*. New York: Academic Press; 1981:562-628.
- Singh M, Brechner R, Horne C. Single photon imaging at high energies with electronic collimation. *SPIE* 1986; 671: 184-188.